IEEE Access
Multidisciplinary ⋮ Rapid Review ⋮ Open Access Journal

Received 22 December 2022, accepted 2 February 2023, date of publication 8 February 2023, date of current version 14 February 2023.

Digital Object Identifier 10.1109/ACCESS.2023.3243251

RESEARCH ARTICLE

Rotor Wake Investigation Under Autorotation Condition in Water Tunnel

LIANG LI[1], FANG WANG[2], MING CHEN[2], MEILIWEN WU[3], ANAN XU[1], AND YONGXI GAO[4]

[1]School of Aeronautic Science and Engineering, Beihang University, Beijing 100191, China
[2]Institute of Unmanned System, Beihang University, Beijing 100191, China
[3]CAAC Key Laboratory of General Aviation Operation, Civil Aviation Management Institute of China, Beijing 100102, China
[4]China Helicopter Research and Development Institute, Jingdezhen 333001, China

Corresponding author: Fang Wang (buaaairforce@buaa.edu.cn)

This work was supported in part by the National Key Research and Development Project of China under Grant 2021YFC3002105, in part by the Key Laboratory of Ministry of Education in Beihang University, and in part by the Helicopter Research Laboratory.

ABSTRACT This paper focuses on the wake features of autorotation status mainly including the induced velocity and tip vortex trajectory in order to preliminary explanation the principle of rotation. In this work, the flow features of autorotating rotor were investigated in water tunnel via particle image velocimetry (PIV) technique. The experiments were conducted with a two-blade single rotor which can freely rotate. The stable rotational speed with various pitch and shaft backward angle was recorded and analyzed. The results show that there is a threshold value of stable rotational speed at shaft backward angle and an optimal region at pitch angle. The PIV results showed that the velocity of the internal wake was much lower than the external, indicating a consuming of energy from the flow, which was in accord with momentum theory. The vortices have three prominent parts: tip vortices, wake sheets and root vortices. There is no apparent interference between wake sheets and tip vortices. The vorticity of the tip was observed to increase in near wake due to lesser interference with the sheets. The Beddoes's model was employed to calculate the tip vortex location with respect to the rotor. The experimental results are in good agreement with the calculated results. It is meaningful for the study to enrich the autorotation theory of rotor and develop underwater rotorcraft.

INDEX TERMS Rotor autorotation, water tunnel, particle image velocimetry, flow feature, wake boundary.

I. INTRODUCTION

Rotorcraft is the most popular product. It maybe be used for Mars or underwater exploration in the future [1], [2], [3], [4], [5]. The performance of rotors is quite complex. A rotor of different states has different characteristics, such as under normal working state, vortex ring state, turbulent wake state and windmill brake state [6]. A rotor, driven or not driven by motor, differs a lot based on principles of motion. Rotor wake interferes greatly with other components, carrying much complex flow than fixed wing. The aerodynamic interference of coaxial helicopters is more complex The autorotation is a very important state in rotor machines, which is the mechanism of autogiro and helicopter autorotative glide [7]. However, the autogiro seems to be half-forgotten and occupies a lower position in the history of aviation [8]. The autogiro was developed by Juan de la Cierva [9], [10] in 1920s, which introduced the mature age of rotorcrafts. The autogiro faded out to general area only when the mature powerful single rotor helicopter mounted the historical stage. No wander most of the researches about autorotation were in early 20th century. In this period, researchers conducted full-scale wind-tunnel tests for autogiro rotor and whole plane model [11], [12]. Most of the mechanism of autorotation had been solved out. The lift, drag, and moment performances changed with tab and stabilizer angle were also concluded. Researchers extracted calculation methods through the autogiro aerodynamics studies [13]. A comparison of calculated and experimental results showed that most of the rotor characteristics could be calculated with reasonable accuracy [14], which was the foundation of rotor theory.

The associate editor coordinating the review of this manuscript and approving it for publication was Norbert Herencsar.

However, because of the old age, most of the researches were unsatisfactory in a modern research sight. With technics developing, the performances of autorotation can be better demonstrated. The wake features of autorotation rotors have never been looked at in detail. Rotor wake is dominated by strong vortices that form and trail from each blade tip [15]. The position and strength of these vortices affect rotor performances, blade loads, and acoustics [16]. Although the gross features of the rotor wake and their influences on power are known, many smaller, but consequential, details are not clearly understood [17], such as the wake sheet geometry and its evolution [18]. It is remarkable that the autorotation, which distinguishes the rotor disc with driving region, driven region, and stall region [19], has an imaginable complex wake geometry, and needs to be given attention. The autorotation state of rotor can also be applied under water, making so called autonomous underwater vehicle [20], [21], [22], which is another meaning for this water tunnel experiments. Underwater vehicle had attracted the attention of many scholars [23], [24], [25], [26], [27], [28].

Additionally, PIV is a very mature technique developed since 1970s, specializing in investigating flow features quantitatively. PIV had been widely used in engineering research [29], [30]. Yu et al. investigated the induced velocity and flow feature of coaxial rotor in both hovering condition and forward flight condition in water tunnel via PIV [31], [32]. They compared the flow feature of coaxial rotor with single rotors in detail. With three-component PIV developing, flow features of full equipped helicopter can be comprehensively investigated with multiply plane of observation windows [33], [34], [35], [36]. Stack et al. [37] conducted an experiment on a three-bladed rotorcraft model in two water tanks to study the flow characteristics of the rotorcraft operating in or near the vortex ring state in descent. Green et al. [38] measured of the flow field around a model rotor descending axially into its own vortex wake using particle image velocimetry.

In this paper, the stable rotational speed and wake features of autorotating rotor were investigated in water tunnel via particle image velocimetry (PIV) technique. In the experiment, PIV 2D plane messages were recorded. The stable rotational speed at various pitch angles and shaft backward angles was recorded and studied. Focusing on two conditions, the critical plane of flow direction and perpendicular direction of flow was analyzed to reach the main vortex feature and velocity feature of the wake. The Beddoes's model is adapted to calculate the tip vortices position with respect to the rotor and compare it with the experimental results. The principle of autorotation was also proved in experiments. This paper gives a better look at the autorotation phenomenon.

II. EXPERIMENT SETUP

A. WATER TUNNEL AND ROTOR SYSTEM

The experiments were carried out in the low-speed water tunnel of Key Laboratory of Ministry of Education in Beihang University. As shown in FIGURE 1, the water tunnel was in a closed loop form which had the main test section of $1.2\times\ 1.0\ \times\ 16m^3$ with a turbulence intensity of about 0.3%. The walls of the test section were made by glass with good light transmission. The maximum velocity of the test section was approximately $0.366m/s$ and the minimum velocity was about $0.1m/s$. The testing water temperature was about 20°. The tracer particles are hollow glass beads with silver plating on the surface. The density of the particles is close to the water density of about $1g/cm^3$, the diameter of the particles is about $5\sim20\mu$m and a surface reflectivity of more than 80%, with good water flow field followability.

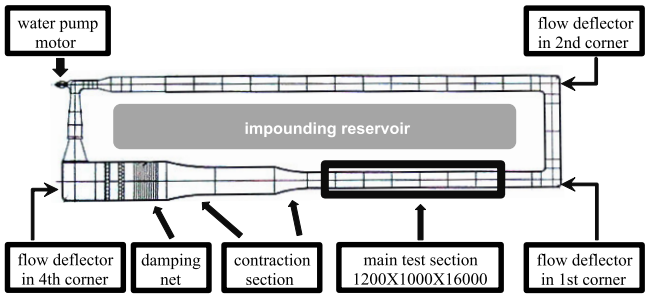

FIGURE 1. Configuration of water tunnel.

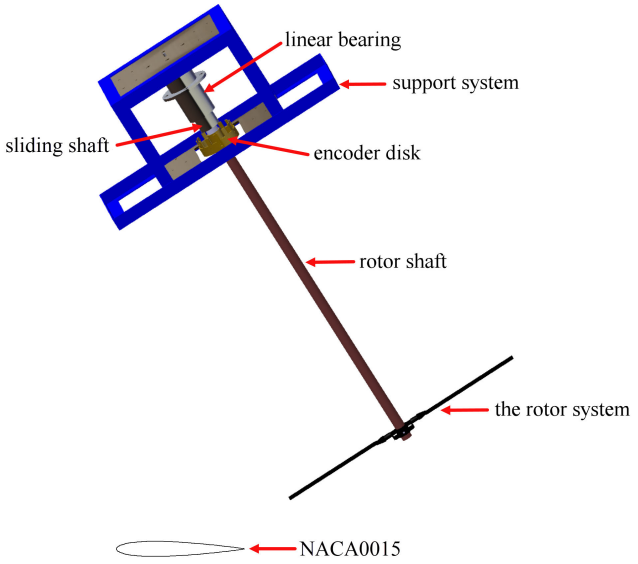

FIGURE 2. View of the test model.

The test model consists of rotor system, rotation system and support system, as shown in FIGURE 2. The main part of the rotor system was a two-blade single rotor. The rotor was able to rotate freely in the clockwise direction (seen from above), and its rotational speed was recorded by an encoder disk fixed on the rotor shaft that shaded the photoelectric switch fixed on the support system. The photoelectric switch recorded the accurate time when the blade rotated to a certain phase position, which was the important reference of wake age. Each blade was untwisted and rigid, which

TABLE 1. Properties of the test rotor.

Rotor type	Hingeless
Number of blades of each rotor	2
Radius	0.25m
Solidity	0.0512
Chord	0.025m
Twist	0°
Root cutout	0.053m
Airfoil	NACA0015

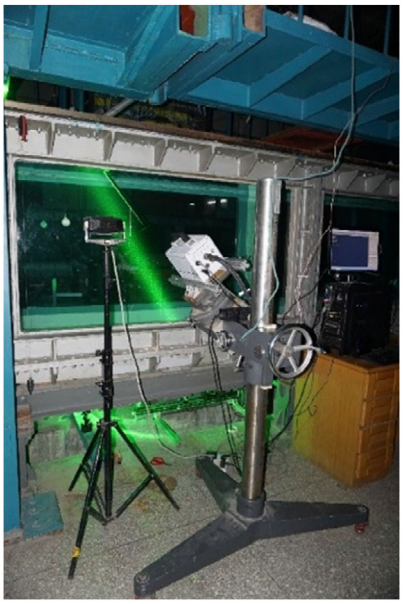

FIGURE 3. The experiment set-up.

was connected rigidly to the hub. The rotor had a radius $R = 0.25\ m$, with a blade root cutout of $0.053m$ (21% of rotor radius). The blade had a rectangular planform and had a chord of $0.025m$. The airfoil was NACA 0015. The detailed rotor properties are shown in Table 1. The surface of the blades was painted black color for reducing reflection. The rotation system consists of rotor shaft, encoder disk and slide shaft. The rotor shaft with 850 mm in length allows the rotor to be positioned in the center of the experimental section of the water tunnel. The encoder disk fixed on the rotor shaft has 12 evenly distributed triggers to indicate the position of the blade. The position of the rotor is recorded by a photoelectric switch fixed to the slide shaft. The slide shaft does not rotate, but can slide up and down along the linear bearing, thus transmitting the rotor thrust to the tension sensor. The support system consists of linear bearing and iron frame. Linear bearing supports the slide shaft to eliminate the bending moment and reduce the slide friction to ensure the accuracy of the thrust measurement. The frame is fixed on a variable angle structure to adjust the shaft backward angle.

In the rotor system, there were two parameters that could be changed. One was the collective pitch, the other was the shaft

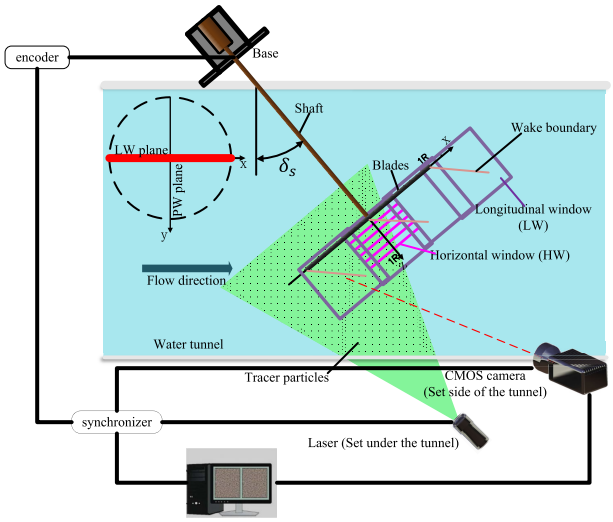

FIGURE 4. Longitudinal window set-up.

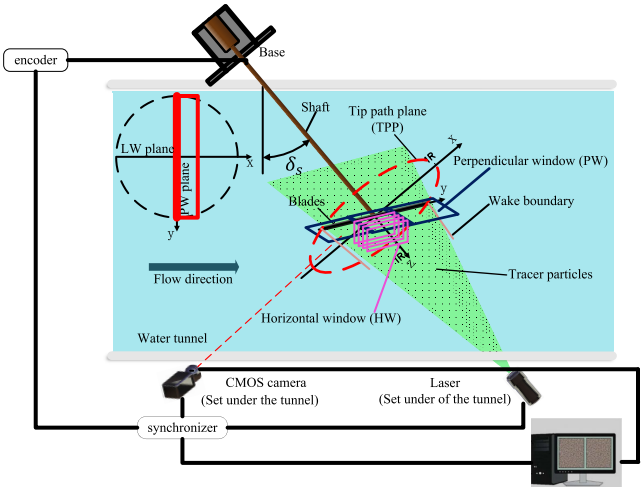

FIGURE 5. Perpendicular window set-up.

backward angle. The shaft backward angle could be changed from $-60°$ to $60°$.

B. PIV INSTRUMENTATIONS

FIGURE 3 shows the whole PIV system and the rotor setup configuration. The whole system consisted of a pair of frequency doubled Nd: YAG lasers, an optical arm, light-sheet optics, a digital CMOS camera of 2048 × 2048 pixels resolution, a high-speed frame grabber, image acquisition and analysis software, and a computer. The fiber optic light arm transmitted the laser light from the dual Nd: YAG lasers to the rotor flow field. The lasers lighted an observation plane in the wake, by emitting a 1mm thickness light sheet.

As shown in FIGURE 4 and FIGURE 5, there were two kinds of observation planes, the longitudinal one was determined by the shaft axes and the flow direction, and the perpendicular one was determined by horizontal direction representing the middle plane of the wake approximately.

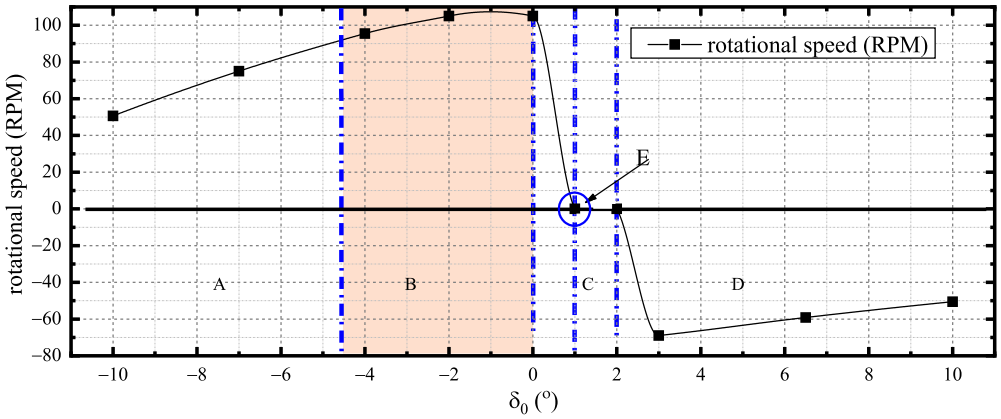

FIGURE 6. The rotational speed changed with δ_0 when $\delta_s = 40°$, $v = 0.366m/s$.

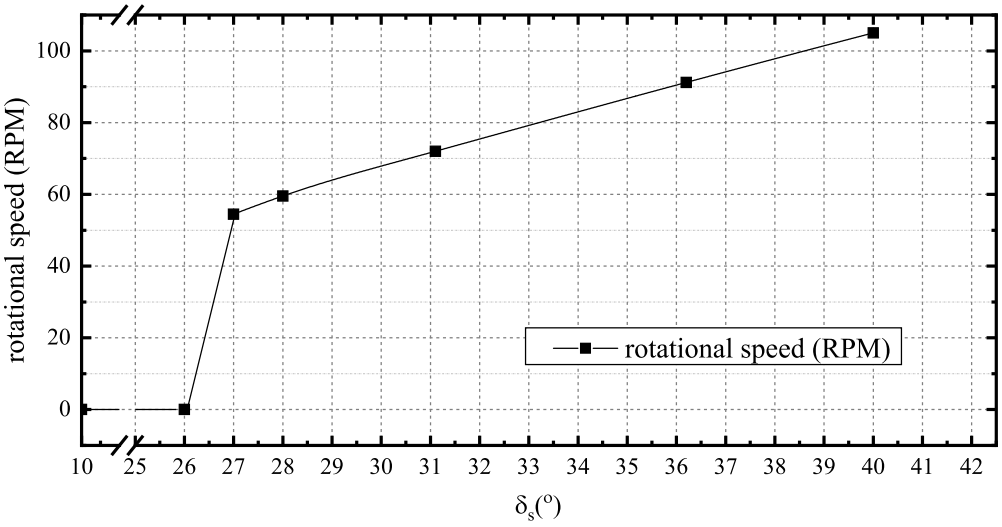

FIGURE 7. The rotational speed changed with δ_s when $\delta_0 = 0°$, v = 0.366m/s.

The longitudinal plane contained the longitudinal window (LW), while the perpendicular plane contained the perpendicular window (PW). These two types of observation planes obtained a spatial view of the wake feature, which got a clear comprehension of the autorotation mechanism. PIV is used to obtain instantaneous velocity measurements and related properties in fluids. The fluid is seeded with tracer particles in the flow field which is illuminated by the laser to illuminate the particles to make them visible and to capture images of them to tack them. The sequential images with tracker particles in motion are then processed for cross correlation to calculate the speed and direction (the velocity field) of the flow which is being observed. Further processing can flow vortices, flow lines and speed lines, and flow field parameters distribution. The synchronizer is connected to the encoder disk trigger, laser launcher, CMOS camera and computer. Once the encoder disk is triggered, the synchronizer sends a signal to the laser to launch light. The CMOS camera captured images of the flow field from a direction perpendicular to the observation plane lit by the laser sheet and stored the data to the computer. The software can display the flow field in real-time.

In FIGURE 4 and FIGURE 5, δ_s meant the shaft backward angle. It was a very important parameter of the autorotation that could influence the rotational speed greatly. The blade's pitch angle δ_0 could also be changed. The positive δ_0 meant that the blade's leading edge rotated downward direction to the bottom of water tunnel, while the negative δ_0 meant that the blade leading edge rotated upward direction to the surface of water tunnel. This was to say, the device was placed upside down in the water tunnel, which had an advantage of avoiding the flow feature being disturbed by the rotating shaft.

III. RESULTS AND DISCUSSIONS

A. ROTATIONAL SPEED FEATURES

The maximum water velocity $v = 0.366m/s$ was selected. δ_0 and δ_s were changed during experiments. It is noteworthy that the system had a relatively fast rotational speed under $\delta_s = 40°$ condition. As shown in FIGURE 6, when $\delta_s = 40°$, the rotor showed differently under different δ_0. In region B,

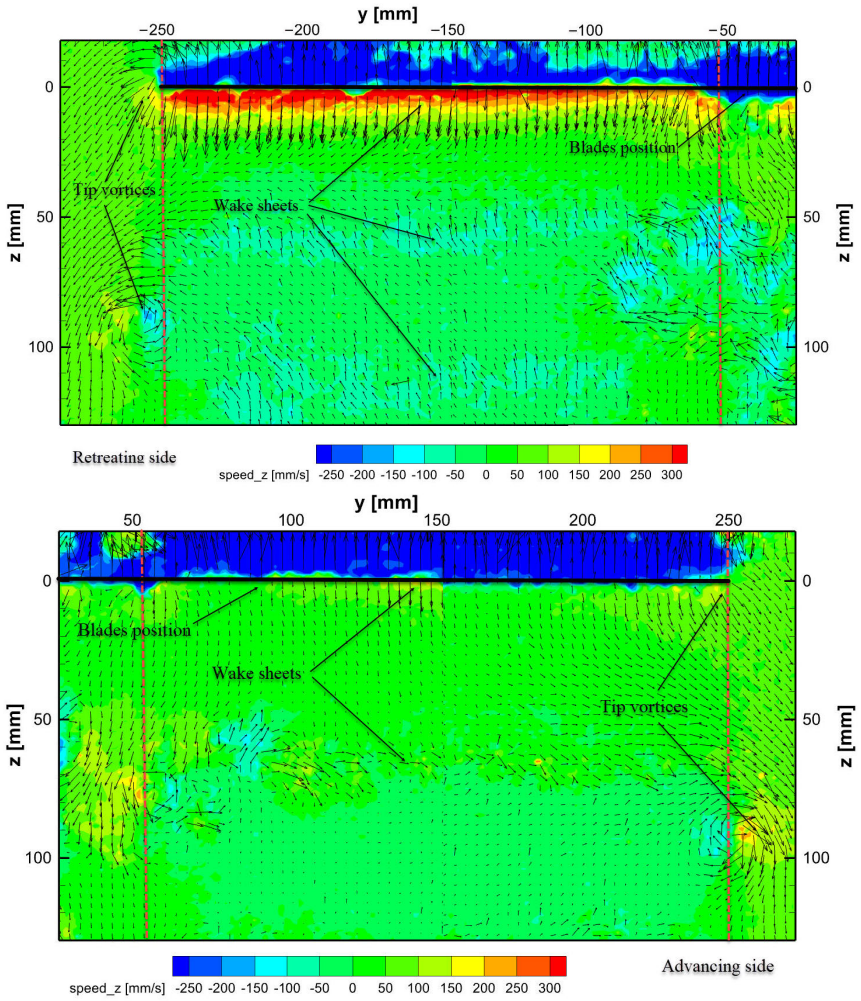

FIGURE 8. Contour of instantaneous induced velocity of Condition No.1 in PW when the blade is at $\psi = 0°$ and 180°.

TABLE 2. PIV experiment conditions.

Condition No.	1	2
δ_0(°)	0	-3
δ_s(°)	40	28
Advance ratio μ	0.28	0.195
External field velocity v(m/s)	0.366	0.366
Autorotation speed in experiment (rad/s)	11.4	7.5
Re	0.71×10^5	0.46×10^5

the rotor rotated fastest in the whole realm, under a stable rotational speed. This was the normal autorotation region. The disc had driving region and driven region at the same time. With δ_0 declined, the rotor rotated slower, as shown in region A. Besides, the rotational speed changed a lot at different phases. This region did not perform normal autorotation, and the driving region occupied most of the disc. The lift contribution of the rotor was limited. At point E $\delta_0 = 1°$, the rotor did not rotate at any δ_s. This was the critical point. At this point the rotate drag was very small. But as δ_0 increased till 2°, the rotate drag increased but the rotor remained static, which identified a critical region C. As δ_0 continued to increase, the rotor rotated inversely, as shown in region D. This region was unnecessary to study. In autorotative glide period of helicopter [19], a $10° \sim 40°$ downward inflow angle (equal to the δ_s) turns out, but not limited to this interval when dealing with urgent situation. In the glide, δ_0 will vary from the highest position to lowest one. Therefore, there is a wide range of autorotation condition that is meaningful to look at in detail. In this work, the region B was the research key point.

FIGURE 7. shows rotation trend when δ_0 was fixed and δ_s was changeable. When $\delta_s > 27°$, the rotational speed was almost in a linear relationship with δ_s. But as $\delta_s < 27°$, the rotor did not rotate.

Two conditions were picked for the PIV experiment to investigate the flow feature in detail as shown in Table 2. The Reynolds number was calculated using the blade chord as the characteristic length.

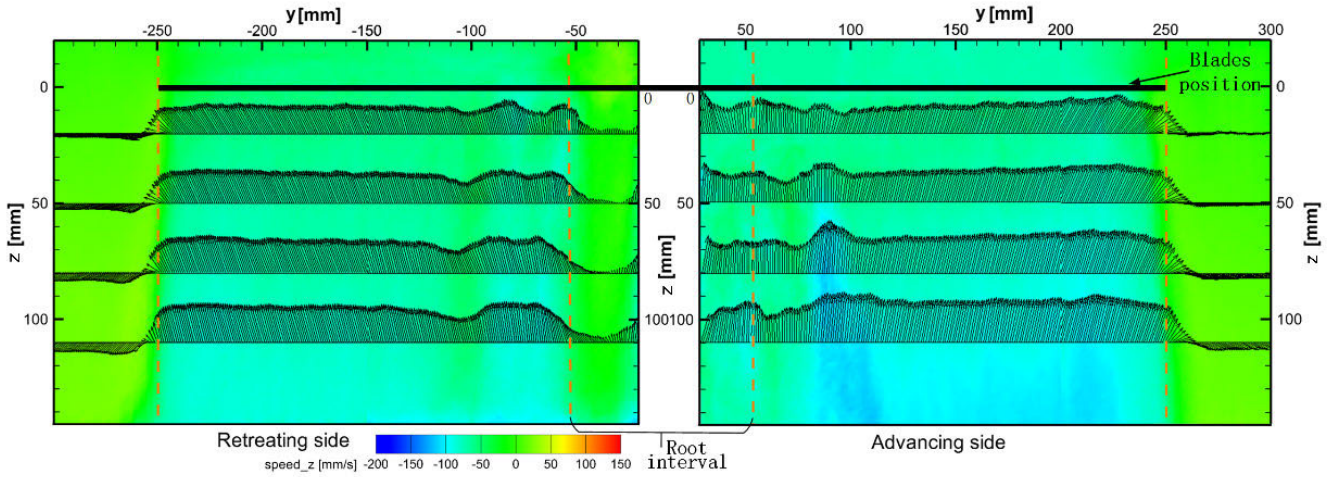

FIGURE 9. Contour of time-averaged induced velocity deduced the external field velocity of Condition No.1 in PW.

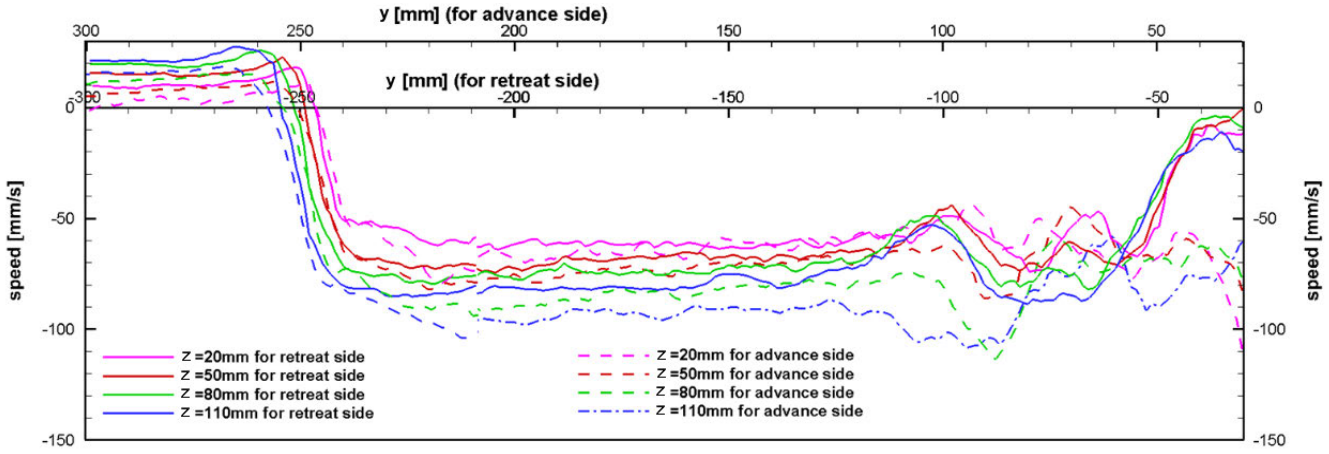

FIGURE 10. Measured time-average spanwise induced velocity distributions in FIGURE 9 at varying axial locations in the wake trailed below rotor in Condition No.1 PW.

B. PIV RESULTS AND DISCUSSIONS

1) PLANE OF CONDITION NO.1

The PW plane recorded the lateral view of the wake, containing both the advancing side and retreating side. The plane showed an extremely clear comparison of the advance-retreat features.

As shown in FIGURE 8, the flow field had a dominant tip vortex, and an associated wake sheet being trailed behind each blade. The rotor had a root cut at $y = 53mm$, so there appeared a considerable strong root vortex. The field region between $[-53, 53]$ influenced by hub and shaft contributed small aerodynamics to the whole rotor, therefore it was not our focus in this paper. To research on the macro features, the time-averaged velocity field was calculated as shown in FIGURE 9. It is noticeable that the velocity inside the wake was much slower than the outside, and the velocity of advancing side was slightly slower than the retreating side according to the darker contour color. In order to have a close view on the velocity differences of the both sides, the spanwise velocity distributions at four equidistant axial locations were extracted in FIGURE 10. With increasing of the axial location, the inner flow of both sides was decreased observed inside the view-window of $z = [150, 0]$. Averagely, the velocity of advancing side was about 15mm/s lower than the retreating side.

To explain the velocity feature of this experiment, the principle of autorotation movement should be considerable. For normal powered rotor, the rotor is drove by engine. While the rotor in autorotation condition is drove by flow field. FIGURE 8-10 show that after the water flowed through the rotor plane, the velocity decreased, which meant the power of the flow lowered and the lost power transmitted to rotation energy. The rotor was driven by water and autorotated in a stable rotational speed.

Because the device was set upside down in the water tunnel, the lift created by rotor pointed to downside in accord with positive z axis. The induced velocity v_i had a direction of negative z. According to the momentum theory [6], the

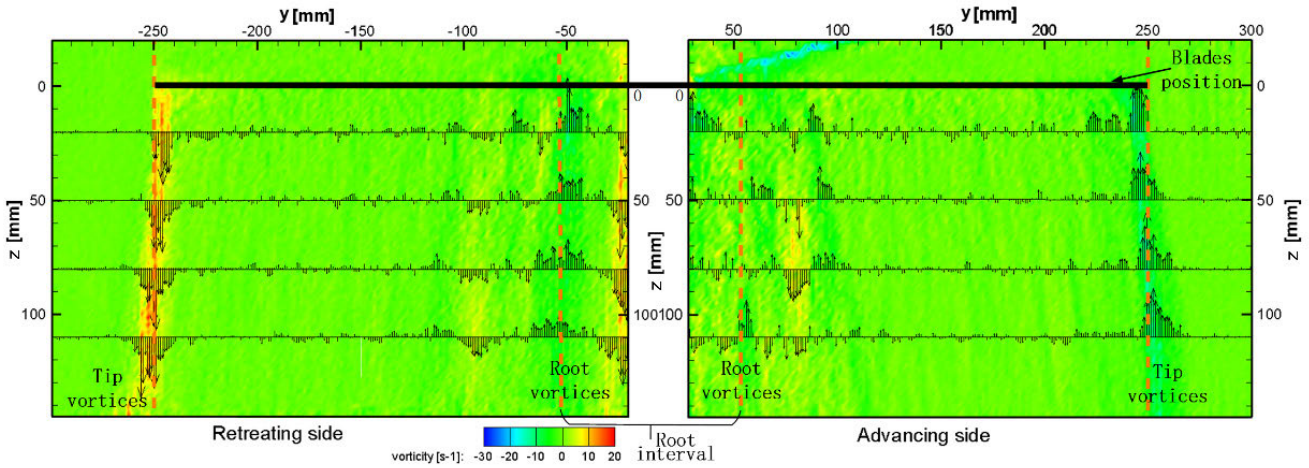

FIGURE 11. Contour of time-averaged vorticity in Condition No.1 PW.

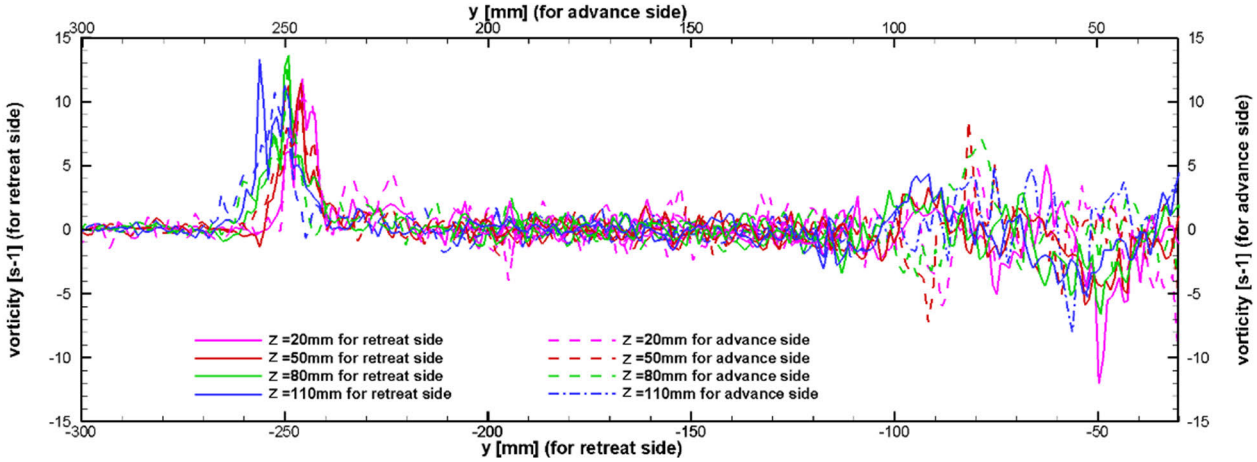

FIGURE 12. Measured time-average spanwise vorticity distribution in FIGURE 10 at varying axial locations in the wake trailed below rotor in Condition No.1 PW.

induced slipstream velocity far away (ω) equals to double the induced velocity v_i at rotor plane, which is also in accord with the experiment result. The lift of the rotor can be estimated as:

$$T = \dot{m}\omega = 2\rho A(V_{inflow} - v_i)v_i \tag{1}$$

Because field messages at 0°, 90°, 180°, and 270° phase position were obtained. Approximately an average induced velocity of these positions was calculated, $v_{i\_ave} = 110mm/s$. Thrust was achieved $T = 10.5N$ by using equation (1), without considering the root lost, tip lost, and induced velocity nonuniform. The calculated thrust coefficient C_T is 0.0132. Compared with the experiment result $T = 8.5N$, the experiment thrust coefficient C_T is 0.0107. It was known that momentum theory can predict the aerodynamics to a certain degree, more importantly it explained the motion principle.

Additionally, it is noticeable that the field was different between the advancing side and retreating side. The rotor aerodynamic distribution was asymmetric in forward flight. As the advance ratio increased, the retreating side grew greater in a disadvantage condition and the asymmetric situation worsen [39]. In FIGURE 9, the color of the advancing side was darker than the retreating, which meant the flow consume more energy and create more lift in advancing side. This difference can be marked as the difference of average induce velocity,

$$\frac{v_{i\_retreat}}{v_{i\_advance}} = 81\% \tag{2}$$

where, $v_{i\_retreat}$ is the average induced velocity on the backward side of the blade, $v_{i\_advance}$ is the average induced velocity of the advancing side of the blade.

FIGURE 11 and 12 quantify the vorticity condition of Condition No.1 in PW. The root vortices occurred at $y = 53mm$. Notice that there were sinusoidal wave-like [40] convections in interval [53, 100] both in advancing and retreating side, which could be concluded as resulted by a kind of interference with the root vortices and spreading. The wake sheets trailed behind a rotor blade consisted of small pairs of coun-

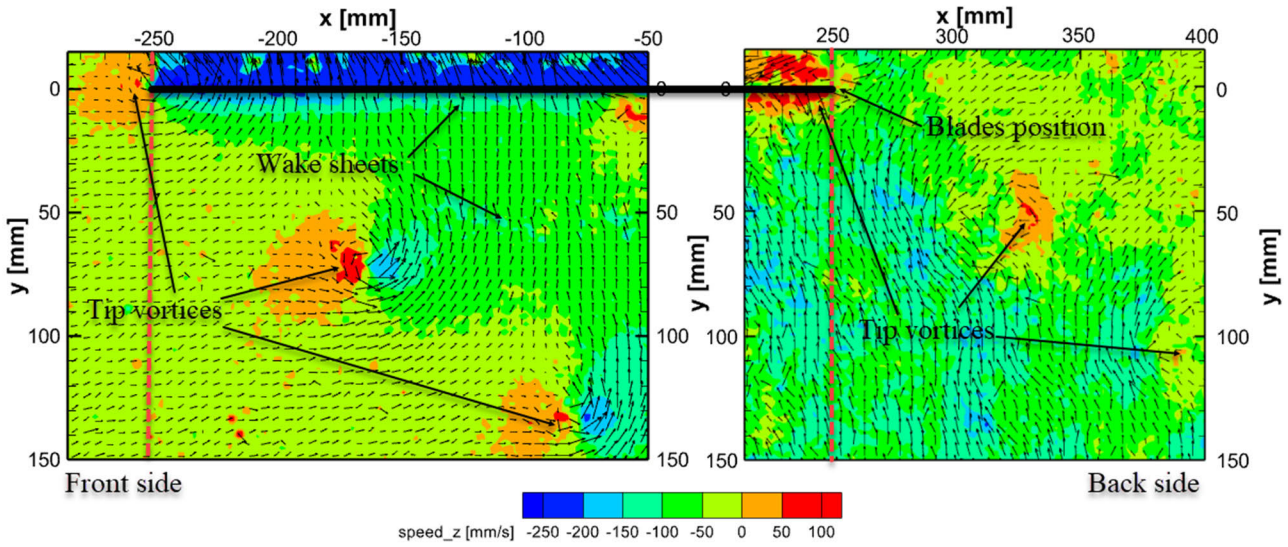

FIGURE 13. Contour of instantaneous induced velocity of Condition No.1 in LW when the blade is at $\psi = 90°$ and 270°.

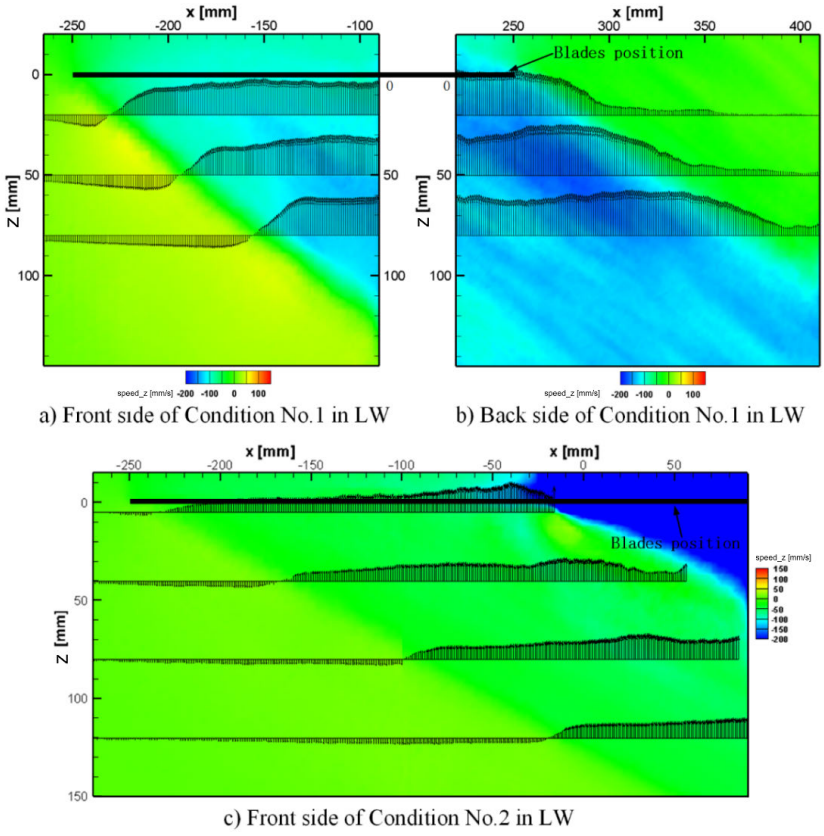

FIGURE 14. Contour of time-averaged induced velocity deduced the external field velocity in LW.

terrotating vortices [41], usually known as T-G vortices [42]. The larger regions of concentrated vorticity indicated tip vortices. The tip vortices and wake sheets developing in this autorotation were unique compared to the normal forward flight condition. First, due to the negative direction of induced velocity, the wake sheets moved downward slower than tip vortices, which was contrary to forward flight powered condition. In this autorotation, the blade and tip vortices interference were nonexistent. Observed a slightly increasement in the strength of the tip vortices inside the view-window of

TABLE 3. Wake skew angle in LW as shown in figure 14.

Condition No.	1	2
Wake skew angle χ /deg	55.2	65.6

TABLE 4. RMS of the TIP vortex trajectory.

Parameter	RMS
x/R (μ=0.128)	0.028
x/R (μ=0.128)	0.056
x/R (μ=0.128)	0.031
x/R (μ=0.128)	0.025

z = [150,0]. This phenomenon could be explained that the distance between the tip vortices and wake sheets increased which lowered the interference and enhance the vorticity at the tip. The vortices moved slower at the advancing side, which made the tip interfere with both the same lap wake sheet and last lap wake sheet, lowered the total strength compared with retreating side. But imaginable, the increasement phenomenon just occurs at a certain axial distance, the vortices are doomed to disappear far away.

2) LW PLANE OF CONDITION NO.1 AND NO. 2

The LW plane recorded the longitudinal view of the wake, containing both the front side and back side. The plane showed an extremely clear comparison of the front-back features.

As shown in FIGURE 13, the front side flow field had a dominant tip vortex, and an associated wake sheet being trailed behind front blade; but the back side flow field influenced by hub and blade had recessive tip vortex and wake sheet. The field region between [−53, 200] had no obvious flow field and wake, therefore it was not our focus in this paper. To research on the macro features, the time-averaged velocity field was calculated as shown in FIGURE 14. It is noticeable that the velocity inside the wake was much slower than the outside, and the velocity of front side was faster than the back side according to the darker contour color. Similar to the PW plane's tip vortices mentioned in the previous chapter, the tip vortices in LW plane were no need to repeat analysis.

Rotor in No.2 Condition created little lift, the condition was not very helpful for engineering application, while the wake could be compared between these two conditions in LW.

C. TIP VORTEX TRAJECTORY

There are several blade tip vortex models [43]. In this study, Beddoes's model [44] is employed since it agrees rather well with experiments. Beddoes's model includes symmetrical roll-up of the blade tip vortex and reflects the asymmetrical roll-up structure of the blade tip vortex.

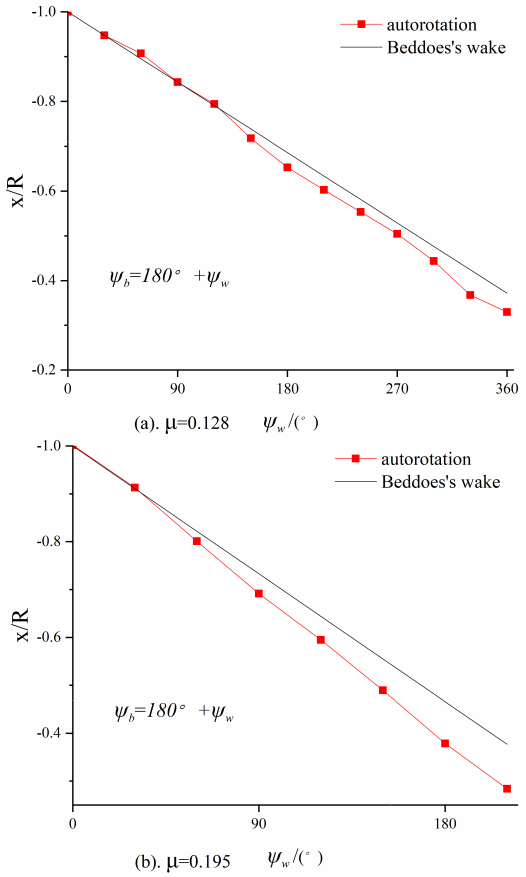

FIGURE 15. The horizontal (radial) displacements of the tip vortices with ψ_b = 180°.

The Beddoes's model is explained below since it is the realistic of the above prescribed wake models by considering conservation of momentum and asymmetry of downwash in the horizontal direction.

The vortex trajectory projection to the x–y plane is assumed as a simple epi-cycloid, and the x–y coordinate is expressed as

$$\frac{x}{R} = cos\,(\psi_b - \psi_w) + \mu\psi_w \tag{3}$$

$$\frac{y}{R} = sin\,(\psi_b - \psi_w) \tag{4}$$

where R is radius of rotor, ψ_b is blade azimuth angle, ψ_w is wake age, μ is rotor advance ratio.

The z coordinate of the tip vortex is given by

$$\frac{z}{R} = -\mu_z\psi_w + \int_0^{\psi_w} \lambda d\psi_b \tag{5}$$

The second term on the right-hand side of the equation basically depends on the value of $cos\,(\psi_b - \psi_w)$. There are three conditions to determine the results of the second term. On the basis of these equations, the three components of the tip vortex location with respect to the rotor can be calculated.

In FIGURE 15, the x/R locations were plotted along a centerline plane at the wake age ψ_w associated with the

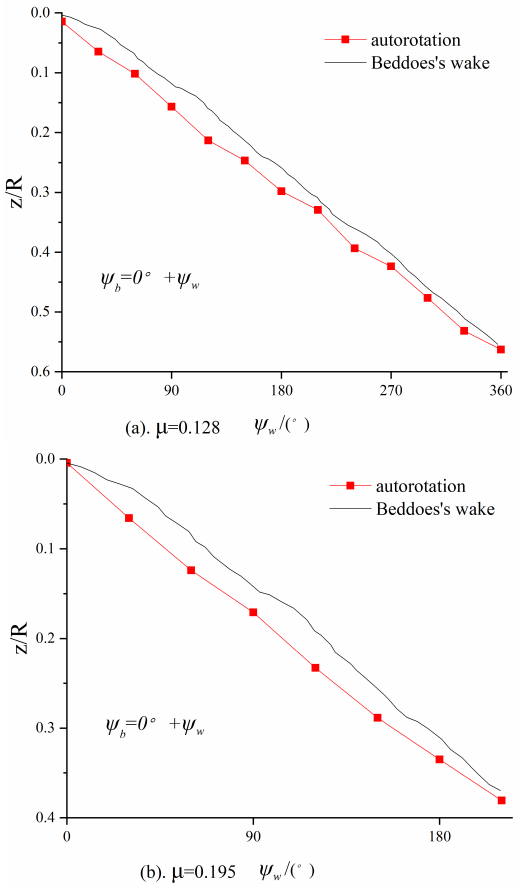

FIGURE 16. The vertical (axial) displacements of the tip vortices with $\psi_b = 180°$.

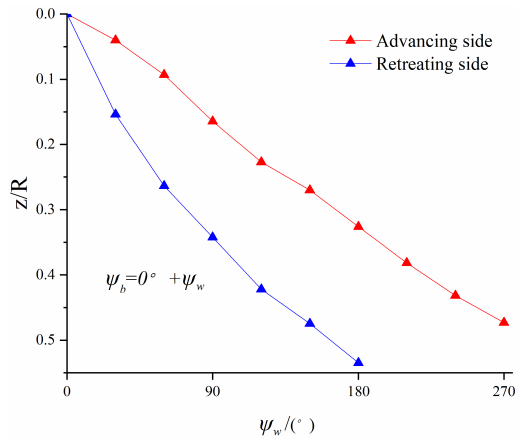

FIGURE 17. The vertical (axial) displacements of the tip vortices with $\psi_b = 90$ and 270°, $\mu = 0.10T$.

intersection of the tip vortex shedding from the leading edge and the trailing edge of the rotor, respectively. The curves of the autorotation rotors are relatively straight especially. As shown in FIGURE 15, the autorotation rotors wake results agree better with the rigid wake model.

In FIGURE 16, the z/R locations were plotted along a centerline plane at the wake age ψ_w associated with the intersection of the tip vortex shedding from the leading edge and the trailing edge of the rotor, respectively. Additionally, Beddoes's generalized wake mode was added for comparison. By comparisons between FIGURE 15 and 16, Beddoes's wake model seemed to have a good agreement with the measurements of this test.

As shown in FIGURE 17, it is noticeable that the wake velocity advancing side was slower than the retreating side, which is the obvious difference between a helicopter and an autorotation rotor.

In the paper, the root mean square value (RMS) is taken to evaluate the errors between the Beddoes's modeled and experimental values of the tip vortex trajectory. The RMS values was used to describe the quantitative index. A computational method of the RMS for the errors $\xi(t)$ is

$$RMS_\xi = \sqrt{\frac{1}{T}\int_0^T \xi^T(t)\xi(t)dt} \tag{6}$$

The quantitative results are summarized in Table 4, which can clearly suggest the Beddoes's model can predict the tip vortex trajectory.

IV. CONCLUSION

PIV measurements were conducted for better understanding the fluid dynamics of autorotation wake. The following conclusions have been drawn from this work:

1) The stable rotational features of autorotation rotor in water tunnel were investigated. The stable rotational speed variation is dramatic when one of shaft backward angle or pitch angle is constant and the other is variable. In this experiment, there is a shaft backward angle threshold for the stable rotational speed. [−4,0] was the best interval of pitch angle for this experiment.

2) The induced velocity in the autorotation wake was much lower than the outside, which was the result of energy absorption principle of autorotation. The experiment phenomenon fitted the momentum theory basically. The calculation results of rotor thrust are compared with the experimental results to preliminary explain the principle of rotation.

3) The rotor wake has some distinctive features. It contained strong tip vortices, wake sheets trailed behind the blade, and root vortices convections. There was no apparent interference of wake sheets and tip vortices in this experiment. The enhancement of vorticity in observation window is attributable to less interference between tip vortices and wake sheets.

4) The Beddoes's model was employed to calculate the tip vortex location with respect to the rotor. The experimental results are in good agreement with the calculated results. The slower wake velocity on advancing side than on retreating side is the obvious distinction between helicopter and autorotation.

5) All our preliminary results throw light on the rotor wake of underwater autorotating rotors. A limitation of this study is that a comparative test was not performed on various airfoil shapes. Future research should focus on performance

calculation based on free wake theory and CFD simulation based on N-S equation to enrich the theory of underwater autorotating rotors.

ACKNOWLEDGMENT

The authors are greatly appreciative of instructor, Ming Chen for providing model-scale rotor setup and for helping with the experimental methods.

CONFLICTS OF INTEREST

The authors declare no conflict of interest.

REFERENCES

[1] P. V. Patil, M. K. Khan, M. Korulla, V. Nagarajan, and O. P. Sha, "Manoeuvring simulations of autonomous underwater vehicle using quaternion," *Defence Sci. J.*, vol. 72, no. 2, pp. 290–307, May 2022, doi: 10.14429/dsj.72.16858.

[2] E. Petritoli and F. Leccese, "Unmanned autogyro for Mars exploration: A preliminary study," *Drones*, vol. 5, no. 2, p. 53, Jun. 2021, doi: 10.3390/drones5020053.

[3] M. Sharma, A. Gupta, S. K. Gupta, S. H. Alsamhi, and A. V. Shvetsov, "Survey on unmanned aerial vehicle for Mars exploration: Deployment use case," *Drones*, vol. 6, no. 1, p. 4, Dec. 2021, doi: 10.3390/drones6010004.

[4] L. Song, H. Zhang, Y. Liu, Y. Wang, and Y. Yang, "Research on negative-buoyancy autorotating-rotor autonomous underwater vehicles," *Appl. Ocean Res.*, vol. 99, Jun. 2020, Art. no. 102123.

[5] Z. Wang, X. Liu, H. Huang, and Y. Chen, "Development of an autonomous underwater helicopter with high maneuverability," *Appl. Sci.*, vol. 9, no. 19, p. 4072, Sep. 2019, doi: 10.3390/app9194072.

[6] J. G. Leishman, *Principles of Helicopter Aerodynamics*, 2nd ed. New York, NY, USA: Cambridge Univ. Press, 2006.

[7] S. S. Houston and R. E. Brown, "Rotor-wake modeling for simulation of helicopter flight mechanics in autorotation," *J. Aircr.*, vol. 40, no. 5, pp. 938–945, Sep. 2003.

[8] J. G. Leishman, "Development of the autogiro: A technical perspective," *J. Aircr.*, vol. 41, no. 4, pp. 765–781, Jul. 2004, doi: 10.2514/1.1205.

[9] G. A. Tokaty, *A History and Philosophy of Fluid Mechanics*. North Chelmsford, MA, USA: Courier Corp., 1994.

[10] J. D. L. Cierva, "New developments of the autogiro," *J. Roy. Aeronaut. Soc.*, vol. 39, no. 300, pp. 1125–1143, Dec. 1935.

[11] J. B. Wheatley and M. J. Hood, "Full-scale wind-tunnel tests of a PCA-2 autogiro rotor," Langley Memorial Aeronaut. Lab., VA, USA, Tech. Rep. NACA-TR-515, 1935.

[12] D. H. Hickey, "Full-scale wind-tunnel tests of the longitudinal stability and control characteristics of the XV-1 convertiplane in the autorotating flight range," Ames Aeronaut. Lab., CA, USA, Tech. Rep. NACA-RM-A55K21a, 1956.

[13] H. Y. Kim, D. J. Sheen, and S. O. Park, "Numerical simulation of autorotation in forward flight," *J. Aircr.*, vol. 46, no. 5, pp. 1642–1648, Sep. 2009.

[14] J. B. Wheatley, "An aerodynamic analysis of the autogiro rotor with a comparison between calculated and experimental results," Langley Memorial Aeronaut. Lab., VA, USA, Tech. Rep. NACA-TR-487, 1935.

[15] N.-P. Bi, J. Leishman, and G. Crouse, "Investigation of rotor wake interactions with a body in low speed forward flight," in *Proc. 9th Appl. Aerodyn. Conf.*, Sep. 1991, p. 3328.

[16] J. G. Leishman, "Measurements of the aperiodic wake of a hovering rotor," *Experim. Fluids*, vol. 25, no. 4, pp. 352–361, Sep. 1998.

[17] M. Ramasamy, N. Gold, and M. Bhagwat, "Flowfield measurements to understand effect of wake behavior on rotor performance," in *Proc. 28th AIAA Appl. Aerodyn. Conf.*, Jun. 2010, p. 4237.

[18] P. F. Lorber, R. C. Stauter, and A. J. Landgrebe, "A comprehensive hover test of the airloads and airflow of an extensively instrumented model helicopter rotor," in *Proc. 45th Annu. Form Amer. Helicopter Soc.*, Boston, MA, USA, 1989, pp. 281–295.

[19] F. A. Administration, *Rotorcraft Flying Handbook*. New York, NY, USA: Skyhorse, 2007.

[20] C. C. Eriksen, T. J. Osse, R. D. Light, T. Wen, T. W. Lehman, P. L. Sabin, J. W. Ballard, and A. M. Chiodi, "Seaglider: A long-range autonomous underwater vehicle for oceanographic research," *IEEE J. Ocean. Eng.*, vol. 26, no. 4, pp. 424–436, Oct. 2001.

[21] X. Li, M. Zhao, F. Zhao, Q. Yuan, and T. Ge, "Study on hydrodynamic performance of heavier-than-water AUV with overlapping grid method," *Ocean Syst. Eng.*, vol. 4, no. 1, pp. 1–19, Mar. 2014.

[22] D. C. Webb, P. J. Simonetti, and C. P. Jones, "SLOCUM: An underwater glider propelled by environmental energy," *IEEE J. Ocean. Eng.*, vol. 26, no. 4, pp. 447–452, Oct. 2001.

[23] H. Kaushal and G. Kaddoum, "Underwater optical wireless communication," *IEEE Access*, vol. 4, pp. 1518–1547, 2016, doi: 10.1109/ACCESS.2016.2552538.

[24] J. Cao, D. Lu, D. Li, Z. Zeng, B. Yao, and L. Lian, "Smartfloat: A multimodal underwater vehicle combining float and glider capabilities," *IEEE Access*, vol. 7, pp. 77825–77838, 2019, doi: 10.1109/ACCESS.2019.2922171.

[25] H. Ghafoor and Y. Noh, "An overview of next-generation underwater target detection and tracking: An integrated underwater architecture," *IEEE Access*, vol. 7, pp. 98841–98853, 2019, doi: 10.1109/ACCESS.2019.2929932.

[26] S. I. Abdelmaksoud, M. Mailah, and A. M. Abdallah, "Control strategies and novel techniques for autonomous rotorcraft unmanned aerial vehicles: A review," *IEEE Access*, vol. 8, pp. 195142–195169, 2020, doi: 10.1109/ACCESS.2020.3031326.

[27] Q. Zhang, J. Lin, Q. Sha, B. He, and G. Li, "Deep interactive reinforcement learning for path following of autonomous underwater vehicle," *IEEE Access*, vol. 8, pp. 24258–24268, 2020, doi: 10.1109/ACCESS.2020.2970433.

[28] Z. Wang, B. Liu, X. Cui, Y. Li, Y. Yang, and Z. Lyu, "The application of micro coaxial rotorcraft in warfare: An overview, key technologies, and warfare scenarios," *IEEE Access*, vol. 10, pp. 40358–40366, 2022, doi: 10.1109/ACCESS.2022.3166890.

[29] C. Chen, C. Hsieh, P. Chi, C. Lin, C. Weng, and C. Hwang, "High-speed image velocimetry system for rainfall measurement," *IEEE Access*, vol. 6, pp. 20929–20936, 2018, doi: 10.1109/ACCESS.2018.2826520.

[30] J. Li, D.-L. Tan, F. Zhao, and X.-J. Yue, "Research on PIV image matching algorithm of turbulent velocity field based on circular projection," *IEEE Access*, vol. 9, pp. 35681–35690, 2021, doi: 10.1109/ACCESS.2021.3061123.

[31] D. Yan-Min, "PIV measurement of water tunnel for the flow field of a hovering coaxial-rotor," *J. Aerosp. Power*, vol. 22, no. 11, pp. 1852–1857, 2007.

[32] S. Yu and Y. Deng, "PIV measurements in the wake of coaxial-rotor in water tunnel," *J. Beijing Univ. Aeronaut. Astronaut.*, vol. 33, no. 6, pp. 635–639, 2007. [Online]. Available: https://bhxb.buaa.edu.cn/en/article/id/9469

[33] F. De Gregorio, K. Pengel, and K. Kindler, "A comprehensive PIV measurement campaign on a fully equipped helicopter model," *Experim. Fluids*, vol. 53, no. 1, pp. 37–49, Jul. 2012.

[34] P. Mortimer, J. Sirohi, S. Platzer, and J. Rauleder, "Coaxial rotor wake measurements in hover using phase-resolved and time-resolved PIV," in *Proc. Vertical Flight Soc. 75th Annu. Forum*, 2019, pp. 13–16.

[35] Y. Ma, M. Chen, X. Zhang, and Q. Wang, "Scale-model tests of coaxial rotors in water tunnel via particle image velocimetry technique," *Proc. Inst. Mech. Eng., G, J. Aerosp. Eng.*, vol. 230, no. 3, pp. 426–443, Mar. 2016.

[36] L. Li, M. Chen, F. Wang, Z. Wu, and A. Xu, "Numerical simulation and PIV experimental investigation on underwater autorotating rotor," *Aerospace*, vol. 10, no. 1, p. 20, Dec. 2022.

[37] J. Stack, F. X. Caradonna, and Ö. Savaş, "Flow visualizations and extended thrust time histories of rotor vortex wakes in descent," *J. Amer. Helicopter Soc.*, vol. 50, no. 3, pp. 279–288, 2005.

[38] R. B. Green, E. A. Gillies, and R. E. Brown, "The flow field around a rotor in axial descent," *J. Fluid Mech.*, vol. 534, pp. 237–261, Jun. 2005, doi: 10.1017/S0022112005004155.

[39] W. Johnson, *Helicopter Theory*. North Chelmsford, MA, USA: Courier Corp., 1994.

[40] J. Milluzzo and J. G. Leishman, "Fluid dynamics of the helicoidal wake sheets trailed from a hovering rotor," *J. Amer. Helicopter Soc.*, vol. 61, no. 1, pp. 1–17, Jan. 2016, doi: 10.4050/JAHS.61.012002.

[41] M. Ramasamy, B. Johnson, and J. G. Leishman, "Turbulent tip vortex measurements using dual-plane stereoscopic particle image velocimetry," *AIAA J.*, vol. 47, no. 8, pp. 1826–1840, Aug. 2009.

[42] P. Hall, "Taylor–Gortler vortices in fully developed or boundary-layer flows: Linear theory," *J. Fluid Mech.*, vol. 124, pp. 475–494, 1982.

[43] N. M. Komerath, M. J. Smith, and C. Tung, "A review of rotor wake physics and modeling," *J. Amer. Helicopter Soc.*, vol. 56, no. 2, Apr. 2011, Art. no. 022006, doi: 10.4050/jahs.56.022006.
[44] T. S. Beddoes, "A wake model for high resolution airloads," in *Proc. 1st Int. Conf. Basic Rotorcraft Res.*, Triangle Park, NC, USA, 1985, pp. 1–12.

LIANG LI received the M.S. degree in aircraft design from Beihang University, Beijing, China, in 2016, where he is currently pursuing the Ph.D. degree in aircraft design.

He is engaged in the research and development of unmanned helicopters for more than ten years and has rich theoretical and engineering experience. His research interests include helicopter overall design, helicopter rotor dynamics, rotor CFD fluid simulation, and helicopter structural dynamics.

FANG WANG received the Ph.D. degree in aircraft design from Beihang University, Beijing, China, in 2015.

He is the master's Supervisor and the Deputy Director of the Beihang Helicopter Research Institute. He is engaged in the research and development of unmanned helicopters for more than ten years, and has rich experience in research and engineering. His research interests include helicopter structure design and helicopter rotor design.

MING CHEN received the M.S. degree in aircraft design from Beihang University, Beijing, China, in 2016. Since 1992, he has been engaged in the teaching and research of helicopter specialty at Beihang University. He was the Deputy Chief Designer of the first coaxial unmanned helicopter in China. He is a Professor, the doctoral Supervisor, and the Director of the Beihang Helicopter Research Institute. His research interests include helicopter overall design, helicopter structure design, and helicopter rotor design. He is a member of the UAV Professional Committee of China Aircraft Owners and Pilots Association (AOPA), UAV Expert Committee of China Electronics Technology Group Corporation, the UAV Industry Alliance of Beijing Science and Technology Commission, and the National Agricultural Aviation Industry Technology Innovation Strategic Alliance.

MEILIWEN WU received the M.S. degree in aircraft design from Beihang University, Beijing, China, in 2014, and the Ph.D. degree in rotorcraft design from Beihang University, Beijing, China, and Politecnico di Milano, Italy, in 2020.

She has been engaged in aircraft flight dynamics and control for more than five years. Her research interests include helicopter overall design, aircraft flight dynamics, UAV flight control, and civil aviation management.

ANAN XU received the M.S. degree in aircraft design from Beihang University, Beijing, China, in 2017, where he is currently pursuing the Ph.D. degree in aircraft design.

He has participated in the design and flight test of unmanned helicopters for more than ten years and has rich theoretical and engineering experience. His research interests include helicopter overall design, helicopter flight dynamics and UAV flight control algorithm.

YONGXI GAO received the M.S. degree in aircraft design from Beihang University, Beijing, China, in 2018.

He is currently the Engineer with the China Helicopter Research and Development Institute. His research interests include helicopter overall design, rotor aerodynamics helicopter structure design, and helicopter rotor design.